doi:10.1093/jmcb/mjv064
Published online December 18, 2015

Article

Enabling systematic interrogation of protein–protein interactions in live cells with a versatile ultra-high-throughput biosensor platform

Xiu-Lei Mo[1], Yin Luo[1,2], Andrei A. Ivanov[1], Rina Su[1,3], Jonathan J. Havel[1], Zenggang Li[1], Fadlo R. Khuri[4], Yuhong Du[1,*], and Haian Fu[1,4,*]

[1] Department of Pharmacology and Emory Chemical Biology Discovery Center, Emory University School of Medicine, Atlanta, GA 30322, USA
[2] State Key Laboratory of Pharmaceutical Biotechnology, School of Life Sciences, Nanjing University, Nanjing 210093, China
[3] Department of Dermatology, XiangYa Hospital, Central South University, Changsha 410008, China
[4] Department of Hematology and Medical Oncology and Winship Cancer Institute, Emory University, Atlanta, GA 30322, USA
* Correspondence to: Haian Fu, E-mail: hfu@emory.edu; Yuhong Du, E-mail: dyuhong@emory.edu

Large-scale genomics studies have generated vast resources for in-depth understanding of vital biological and pathological processes. A rising challenge is to leverage such enormous information to rapidly decipher the intricate protein–protein interactions (PPIs) for functional characterization and therapeutic interventions. While a number of powerful technologies have been employed to detect PPIs, a singular PPI biosensor platform with both high sensitivity and robustness in a mammalian cell environment remains to be established. Here we describe the development and integration of a highly sensitive NanoLuc luciferase-based bioluminescence resonance energy transfer technology, termed BRET^n, which enables ultra-high-throughput (uHTS) PPI detection in live cells with streamlined co-expression of biosensors in a miniaturized format. We further demonstrate the application of BRET^n in uHTS format in chemical biology research, including the discovery of chemical probes that disrupt PRAS40 dimerization and pathway connectivity profiling among core members of the Hippo signaling pathway. Such hippo pathway profiling not only confirmed previously reported PPIs, but also revealed two novel interactions, suggesting new mechanisms for regulation of Hippo signaling. Our BRET^n biosensor platform with uHTS capability is expected to accelerate systematic PPI network mapping and PPI modulator-based drug discovery.

Keywords: bioluminescence resonance energy transfer, NanoLuc luciferase, protein–protein interaction, Hippo signaling pathway

Introduction

While advances in genomics research have led to critical insights into vital biological processes, how to leverage the enormous datasets for functional understanding of biology, for associating genotype with phenotypic changes in diseases, and for therapeutic intervention remains a daunting challenge (Cancer Genome Atlas Research Network, 2008, 2014a, b, c). To address this issue, it is important to understand various molecular interactions within cells that translate genomic information into functional networks to drive biological or pathophysiological outcomes, for instance protein–protein interactions (PPIs).

A large number of technologies have been developed to detect PPIs and some are applicable for high-throughput screening, including yeast two-hybrid (Rolland et al., 2014), protein fragment complementation assay (Ding et al., 2006; Tarassov et al., 2008), and affinity purification-coupled mass spectrometry (Collins et al., 2013). However, genome-scale detection of PPIs with physiological relevance demands a technology platform that not only offers detection sensitivity and robustness, but also features ease of manipulation to enable automated high-throughput PPI monitoring for quantitative assessment in a live cell environment. Bioluminescence resonance energy transfer (BRET) technology has recently attracted significant attention due to its robust performance that enables quantitative study of PPIs in live cells (Angers et al., 2000; Mercier et al., 2002; Canals et al., 2003; Pfleger and Eidne, 2006). The use of *Renilla* luciferase (RLuc) from *Aequorea* as BRET donor has popularized BRET for live cell PPI monitoring due to its ease of coupling test proteins to RLuc through engineered gene fusions. Different acceptor proteins, typically fluorescence proteins, were coupled with RLuc to generate various BRET biosensors, such as BRET^1 (Xu et al., 1999; Hamdan et al., 2005) and BRET^2 (Ramsay et al., 2002; Vrecl et al., 2004). Although the RLuc-based BRET platform has been widely used in PPI studies, the broad emission spectrum and weak

Received August 10, 2015. Revised October 1, 2015. Accepted October 9, 2015.

luminescence signal of RLuc significantly hinder its further development and application, especially for ultra-high-throughput screening (uHTS) (Couturier and Deprez, 2012).

In this study, we develop and validate a NanoLuc luciferase (NLuc)-based BRET system, termed BRET^n, in 1536-well uHTS format. NLuc is a luminescent protein engineered from the luciferase of a luminous deep-sea shrimp, *Oplophorus gracilirostris* (Hall et al., 2012). It has been shown that NLuc is the smallest (19 kDa) and brightest luciferase to date, with superior stability, glow-type luminescence, and narrower emission spectrum (Hall et al., 2012). Here we utilize BRET^n to analyze individual pairs of interacting proteins in a demanding uHTS format, which includes (i) a chemical library screening for PRAS40 dimer inhibitors in support of chemical biology research and (ii) Hippo signaling pathway profiling for systematic network mapping and novel PPI discovery. Our BRET^n biosensor platform, with capabilities for sensitive detection and quantitative measurement of PPIs in live cells in uHTS format, will allow rapid discovery of small-molecule PPI modulators and PPI networks.

Results

NLuc exhibits enhanced efficiency and superior performance over RLuc as BRET donor

Our BRET^n PPI biosensor design uses NLuc, instead of the conventional RLuc, as a BRET donor. This change leverages the improved properties of NLuc luciferase for superior BRET assay performance. Venus, a yellow fluorescence protein variant, serves as a BRET acceptor. The interaction of NLuc-fused protein X and Venus-fused protein Y brings the donor and acceptor into close proximity, leading to energy transfer of the luminescence signal from NLuc to Venus upon substrate addition (Figure 1A). The emission signal of Venus can then be used as a measurement of BRET signal for detection of PPIs (Figure 1A).

To examine the performance of NLuc luciferase and select the optimal cell-permeable substrate for our study in live cells, we carried out spectrum scanning of the emission signal from NLuc and RLuc using furimazine or ViviRen^{TM} as luciferase substrates in live cells. As shown in Figure 1B, NLuc is indeed >10 times brighter than the conventional BRET donor RLuc when using ViviRen^{TM} as substrate. Using furimazine as substrate for NLuc further increased the emission signal by >2-fold. The detected maximum emission signal was at ~460 nm. In addition, the emission spectrum of NLuc is ~25% narrower than that of RLuc (Figure 1B, inset). Narrow spectra of the donor may reduce signal crossover with the acceptor detection window, leading to a decrease in the BRET background signal. These results indicate that the use of NLuc may increase the sensitivity and specificity of BRET signal for improved PPI detection compared with RLuc. Furimazine was selected and used as the cell-permeable

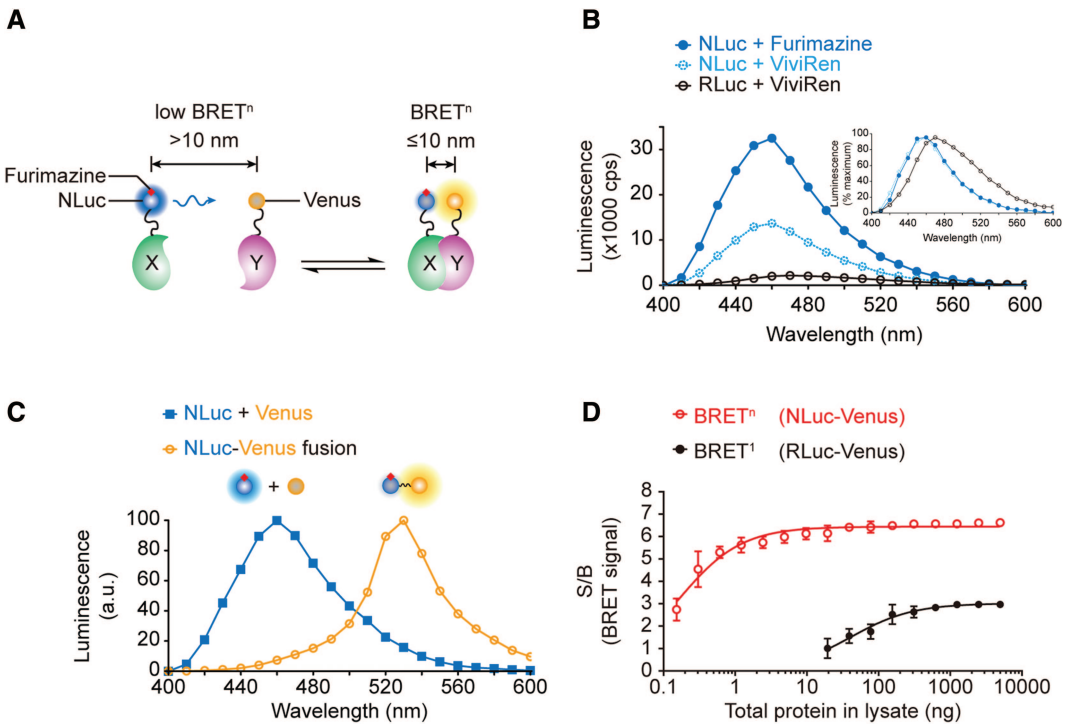

Figure 1 The design and development of BRET^n. (**A**) BRET^n design. NLuc and Venus are genetically fused to the N-terminal end of each protein of interest, X and Y, respectively. BRET signal can be detected when NLuc and Venus are brought into close proximity upon the interaction between proteins X and Y. (**B**) Luminescence spectra of NLuc and RLuc with live cell substrate furimazine and ViviRen^{TM}, respectively. Normalized spectra profiles are shown in the inset. (**C**) Luminescence spectra of live cells expressing NLuc-Venus fusion proteins or NLuc with unfused Venus. (**D**) Comparison of NLuc-Venus with RLuc-Venus fusions. BRET signal window (S/B) from cell lysates containing various amounts of NLuc-Venus or RLuc-Venus fusion are shown. The data are expressed as mean ± SD from three independent experiments.

substrate that was added directly to live cells in all of the following studies.

To employ NLuc/Venus as donor (D)/acceptor (A) pair for BRET, we generated a NLuc-Venus fusion construct as a positive BRET biosensor control and NLuc with unfused Venus protein as a negative control. The constructs were expressed and the spectra were scanned in live cells. As shown in Figure 1C, the maximum emission for cells co-transfected with NLuc with unfused Venus was ~460 nm, while the NLuc-Venus fusion transfection led to a large red-shifted spectrum with the maximal emission at 530 nm. The emission at 460 nm for the NLuc-Venus fusion was minimal. These results indicate that a large proportion of NLuc luminescence energy has been transferred to the fused Venus, supporting the use of NLuc/Venus as an effective BRET donor/acceptor pair for studying PPIs in living cells.

Next, we sought to determine the sensitivity of BRET^n (using NLuc-Venus fusion as an example) and compared it with traditional BRET^1 (using RLuc-Venus as an example). Through titration studies, as shown in Figure 1D, we found that the signal-to-background ratio (S/B) of BRET^n (as for NLuc-Venus fusion) was >2-fold higher than that of BRET^1 (as for RLuc-Venus fusion) at high protein levels. It was apparent that at low range of protein concentrations (1–10 ng), S/B of BRET^n remained high at ~6-fold over the background control whereas S/B of BRET^1 became undetectable. The differential dose-dependent S/B curves clearly demonstrated a superior performance of BRET^n to BRET^1 (Figure 1D). These data indicate that BRET^n has improved sensitivity compared with conventional BRET^1.

BRET^n is sensitive for detection of PPIs at nearly endogenous level

To further examine the sensitivity of BRET^n for PPI detection, the dynamic window of BRET^n was evaluated for measuring dimerization of proline-rich Akt substrate of 40 kDa (PRAS40). We first scanned and compared the emission spectra of live cells expressing PPI protein pairs or background controls. As shown in Figure 2A, the distinction between the signal and background spectra of BRET^n was significantly greater than that of BRET^1. The S/B of PRAS40 dimerization detected by BRET^n is 2-fold higher than that from BRET^1 (Figure 2A, inset).

To test whether such enhanced sensitivity of BRET^n could allow us to detect PPIs at low expression levels, we next measured BRET^n signal for PRAS40 dimerization at a range of PRAS40 protein expression levels. As revealed by western blot analysis (Figure 2B), the NLuc- and Venus-tagged PRAS40 showed a range of expression levels in comparison with the endogenous PRAS40. Significant BRET^n signals could be detected when NLuc-PRAS40 and Venus-PRAS40 were co-expressed, even at endogenous expression levels (lanes 1–3), as compared with NLuc-PRAS40 and Venus control (Figure 2C). Our results demonstrate that the increased sensitivity of BRET^n compared with BRET^1 provides superior assay performance in the setting of low protein expression, which allows the detection of PPIs at physiological expression levels.

Miniaturization of BRET^n into a 1536-well plate to enable uHTS

To explore the potential application of the BRET^n system for systematic study of PPIs in a large-scale setting, we evaluated its feasibility and performance in a 1536-well plate uHTS format.

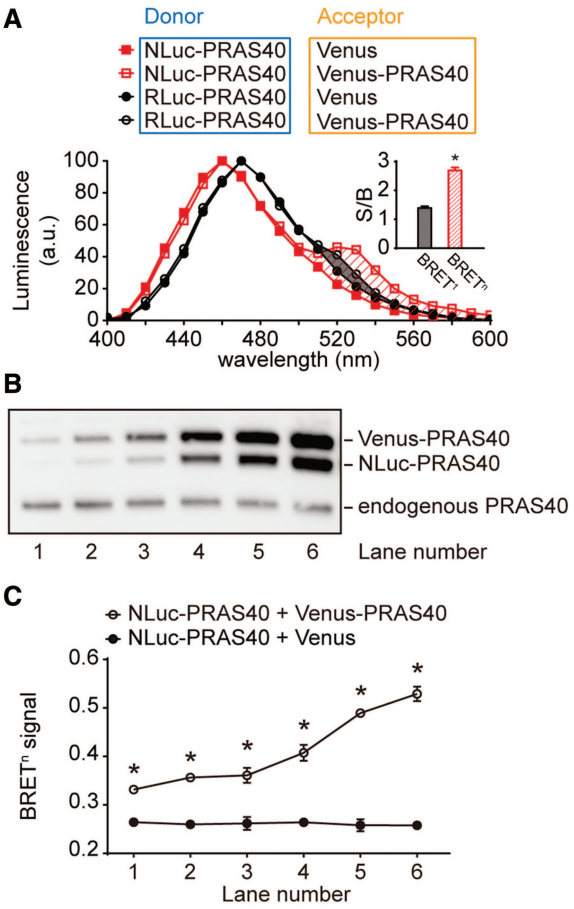

Figure 2 BRET^n allows the detection of PPI at nearly endogenous expression level. (**A**) The detection of PRAS40 dimerization by BRET^n and BRET^1. Normalized emission spectrum profiles of BRET^n and BRET^1 for PRAS40 dimerization are shown. S/B of BRET signal is shown in the inset (maximal CPS for NLuc and RLuc were 30000 and 3000, respectively). (**B**) Expression level of NLuc- and Venus-tagged PRAS40 compared with endogenous PRAS40. HEK293T cells were co-transfected with various amounts of NLuc- and Venus-tagged PRAS40. Whole-cell lysate was used for western blot analysis with anti-PRAS40 antibodies. (**C**) BRET^n analysis. Whole-cell lysate from the same sample as in **B** was added into a 1536-well plate for BRET detection. The data are expressed as mean ± SD from three independent experiments. *$P \leq 0.05$.

First, we performed a titration experiment for the well-studied Raf-1 and 14-3-3σ PPI, with the BRET^n platform in 1536-well format in live cells by varying the amount of transfected donor (NLuc-Raf-1) and acceptor (Venus-14-3-3σ) plasmids. Saturation curve analysis revealed that the BRET signal increased as the Acceptor/Donor ratio increased. The signal reached plateau when the Acceptor/Donor ratio was ≥5 (Figure 3A). To validate the specificity of the BRET^n signal, the interaction between Raf-1 and a charge-reversal mutant of 14-3-3σ, K49E, which is defective

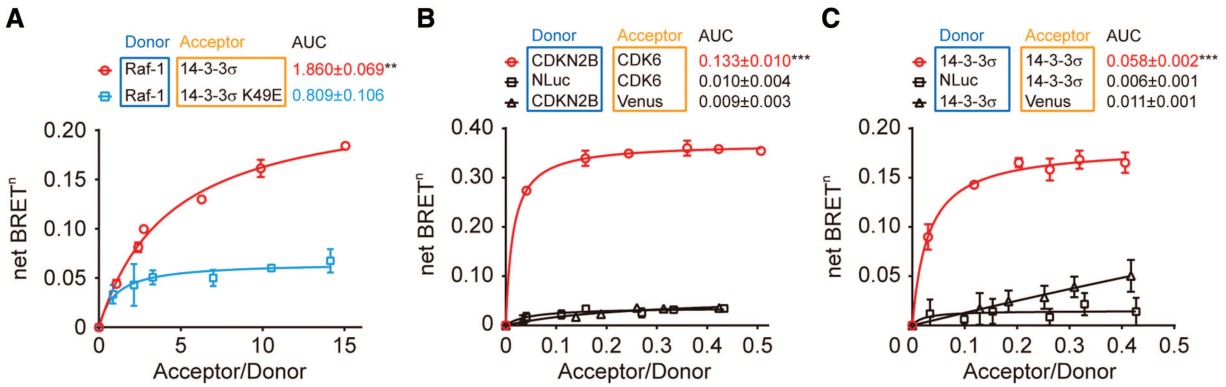

Figure 3 Validation of the miniaturized BRET^n format with known PPIs. H1299 cells were co-transfected with test fusion constructs in a 1536-well plate and BRET^n signals were determined. (**A**) Differential BRET^n saturation curves of Raf-1 interaction with 14-3-3σ and the binding-defective mutant 14-3-3σ K49E. (**B** and **C**) BRET^n saturation curves of additional known positive PPIs, including CDK6/CDKN2B (**B**) and 14-3-3σ homodimerization (**C**). The data are presented as mean ± SD from four replicates. AUC values for PPIs and corresponding controls are listed and presented as mean ± SD from three independent experiments. $^{**}P \leq 0.01$, $^{***}P \leq 0.001$.

in ligand binding, was evaluated. As shown in Figure 3A, the BRET^n signal from the interaction of mutant 14-3-3σ K49E with Raf-1 was significantly decreased. These data confirm the robustness and specificity of the uHTS BRET^n system for PPI detection.

Next, we examined two defined PPIs in different subcellular compartments, i.e. nuclear CDK6/CDKN2B interaction (Hannon and Beach, 1994) and cytoplasmic 14-3-3σ dimerization (Fu et al., 2000). BRET^n saturation studies for the CDK6/CDKN2B interaction (Figure 3B) and 14-3-3σ dimerization (Figure 3C) showed that the BRET^n signal for both PPIs was significantly higher than the background signal for controls. The S/B ratios of AUC values were 5.3 for cytoplasmic 14-3-3σ/14-3-3σ dimerization and 13.3 for nuclear CDK6/CDKN2B interaction. The robust BRET signals from these known PPI pairs demonstrate excellent assay performance of BRET^n in a 1536-well miniaturized uHTS format. The significantly reduced amount of plasmids and reagents required in the miniaturized format enables cost-effective large-scale PPI mapping and PPI modulator discovery. Further, our results suggest that the BRET^n platform can be readily utilized to monitor both cytoplasmic and nuclear PPIs, including 14-3-3σ dimerization, 14-3-3σ/Raf-1, and CDK6/CDKN2B interactions.

uHTS BRET^n enables the discovery of small-molecule PPI modulators in live cells

Given the robust performance of the uHTS BRET^n assay, we tested its feasibility for small-molecule modulator discovery. For this purpose, the NLuc donor/Venus acceptor interaction has to be dynamic in cells for detection of signal disruption by small-molecule PPI inhibitors. As a proof-of-concept, we examined the effect of a known small-molecule PPI disruptor, nutlin-3, on the interaction between TP53 and MDM2, a validated drug target (Vassilev et al., 2004). We first performed titration studies to establish BRET^n saturation curves for the TP53/MDM2 interaction. As shown in Figure 4A, the interaction of NLuc-TP53 and Venus-MDM2 generated a robust signal with the S/B ratio of the AUCs >5. Using this TP53/MDM2 BRET^n biosensor, we were able to capture nutlin-3b-induced dissociation of the TP53/MDM2 interaction in live cells with a half maximal inhibitory concentration of ~17.3 μM (Figure 4B). This result is consistent with previously reported IC_{50} at 13.6 μM for nutlin-3b in an *in vitro* TP53/MDM2 interaction assay using purified proteins (Vassilev et al., 2004). Thus, the BRET^n-based configuration allows reversible detection of binary molecular interactions, as demonstrated by effective inhibition of TP53/MDM2 PPI by its known inhibitor, nutlin-3b. In this manner, our uHTS BRET^n is sensitive for monitoring dynamic changes in PPIs and is ready to be adapted for rapid screening and discovery of small-molecule PPI modulators in live cells.

BRET^n biosensor for discovering small-molecule modulators of PRAS40 dimerization

We next utilized the uHTS BRET^n platform in a small-molecule screening to discover modulators of PRAS40/PRAS40 dimerization. PRAS40 is a prominent AKT substrate and plays important roles in the control of mTOR-mediated pathways, but its regulatory mechanism remains unclear. Discovery of small-molecule chemical probes that modulate PRAS40 dimerization could provide useful tools to unravel the role of PRAS40 in mTOR signaling. We first validated the dimerization of PRAS40 using a GST pull-down assay (Figure 5A). We then established BRET^n saturation curves for PRAS40 dimerization with the S/B ratio of AUC values >17 (Figure 5B) in a uHTS platform. Together, our data from multiple orthogonal assays confirmed that PRAS40 can form homo-dimers and are consistent with the data acquired through AP-MS (Havel et al., 2015).

We carried out a pilot screening with a library of 1600 compounds to validate the assay performance of the developed BRET^n biosensor for PRAS40 dimerization. HEK293T cells with co-expressed NLuc-PRAS40 and Venus-PRAS40 were treated with library compounds and the BRET^n signal in live cells was then measured. The BRET biosensor in uHTS format has robust performance with consistent S/B ratio >3 (Figure 6A) and Z' factor >0.6 (Figure 6B) across five 1536-well screening plates.

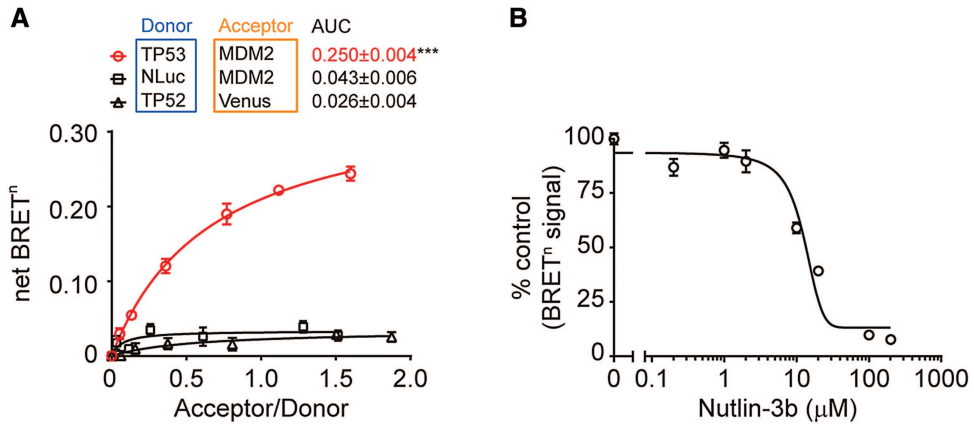

Figure 4 Monitoring of Nutlin-3b-induced dissociation of TP53/MDM2 interaction by BRET^n. (**A**) BRET^n saturation curves of TP53/MDM2 using NLuc-TP53 and Venus-MDM2. (**B**) Dose-dependent decrease of BRET^n signal for TP53/MDM2 with increasing Nutlin-3b concentration. The data are expressed as mean ± SD from four replicates, and HEK293T cells were used. AUC values for PPIs and corresponding controls are listed and presented as mean ± SD from three independent experiments. ***$P \leq 0.001$.

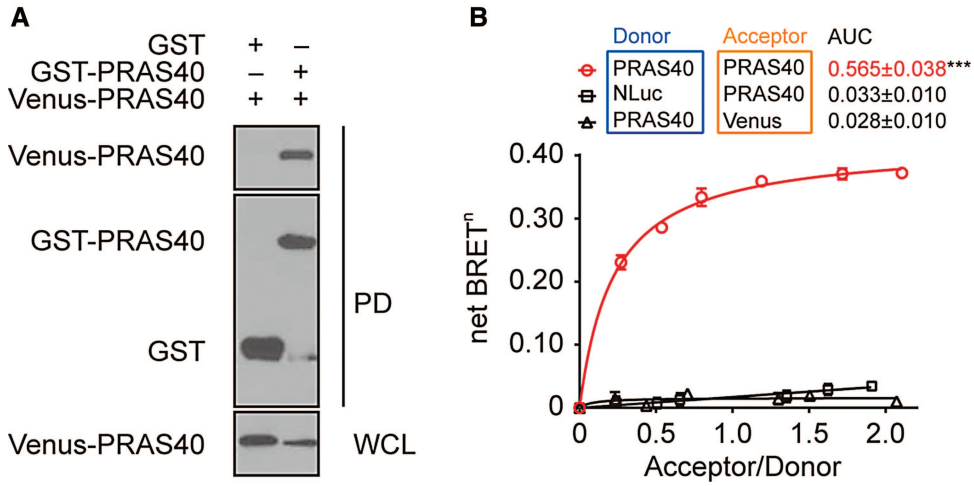

Figure 5 Validation and BRET^n biosensor development for PRAS40 dimerization. (**A**) GST pull-down validation of PRAS40 dimerization in HEK293T cells. (**B**) BRET^n saturation curves of PRAS40 dimerization detected in H1299 cells co-expressed with NLuc- and Venus-tagged PRAS40. The data are expressed as mean ± SD from four replicates. AUC values for PPIs and corresponding controls are listed and presented as mean ± SD from three independent experiments. ***$P \leq 0.001$.

Among the 1600 compounds, 2 hit compounds were identified that decreased the PRAS40 dimerization-induced BRET signal (Figure 6C). One of the hit compounds, p-Chloromercuribenzonic acid (PCMB), was able to decrease the dimerization signal by ~50% at 20 μM (Figure 6C). This PPI disruptive effect was further validated using GST pull-down, where a dose-dependent decrease of Venus-PRAS40 was observed following GST-PRAS40 pull-down (Figure 6D), with an IC_{50} at ~34 μM (Figure 6E). Another hit compound, pararosaniline, could be a false-positive hit, since it also decreased the BRET^n signal of the fusion control NLuc-Venus with similar potency (Figure 6F). These results illustrate the efficiency of the BRET^n biosensor in a uHTS format for rapid screening and identification of small-molecule PPI modulators in live cells.

uHTS BRET^n enables efficient PPI mapping to reveal new pathway connectivity

To apply uHTS BRET^n for rapid PPI mapping, we designed orthogonal experiments that simultaneously monitor multiple bimolecular interactions within one 1536-well plate. The evolutionarily conserved Hippo pathway plays a critical role in normal physiology, such as the control of organ size during development. Its dysregulation has been associated with tumorigenesis in a range of cancer types (Huang et al., 2005; Zhao et al., 2007; Harvey et al., 2013; Johnson and Halder, 2014). Thus, understanding the landscape of the Hippo pathway interactome may facilitate decoding its pathophysiological function and design of approaches for therapeutic interrogation (Couzens et al., 2013; Kwon et al., 2013).

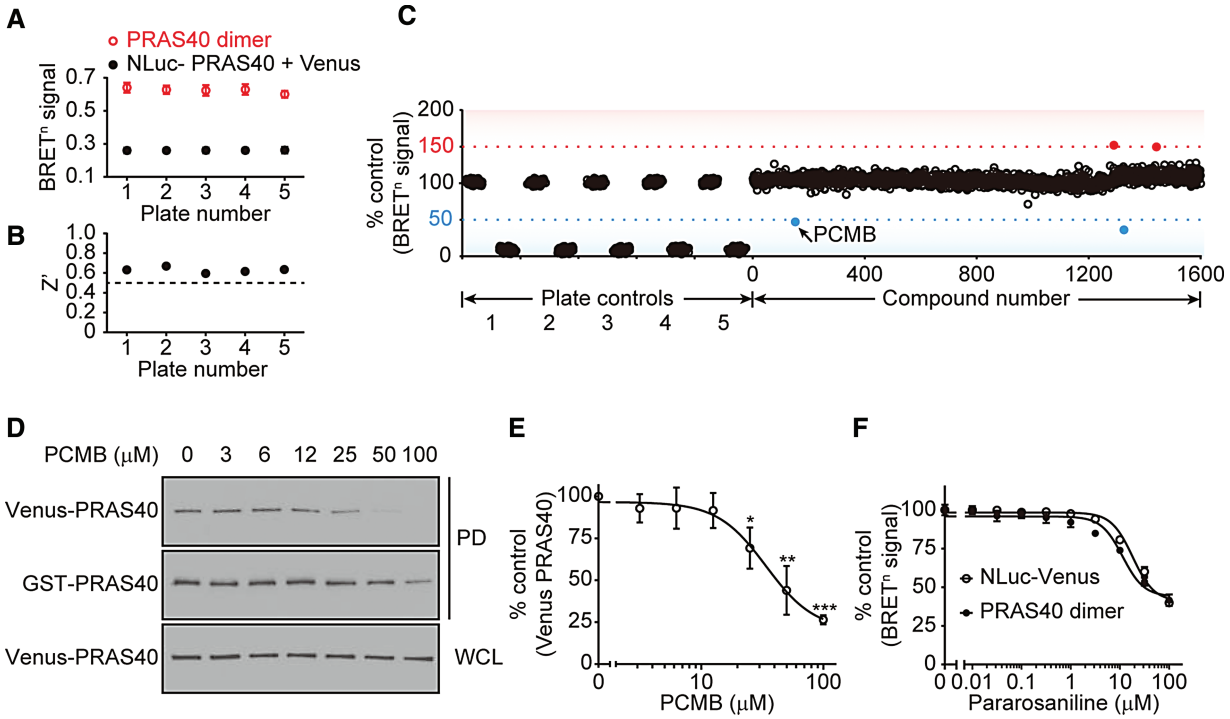

Figure 6 The identification of PCMB as a PRAS40 dimerization inhibitor through BRET^n-based uHTS. (**A** and **B**) BRET signals (**A**) and *Z'* (**B**) from five independent assay plates were used to evaluate the assay performance for uHTS. The data are presented as mean ± SD from 64 replicate wells. (**C**) PRAS40 dimerization inhibitor screening with BRET^n. HEK293T cells expressing NLuc- and Venus-tagged PRAS40 were treated with individual compound at 20 μM for 16 h. A library of 1600 compounds were tested. (**D**) Validation of PCMB disruptive effect on PRAS40 dimerization using GST pull-down. Cell lysate was incubated with various amounts of PCMB for 2 h at 4°C before performing GST pull-down, and then incubated with GST beads for another 2 h. The amount of Venus-PRAS40 in the GST-PRAS40 complex was detected by western blotting with anti-PRAS40 antibodies. (**E**) Dose–response curve of PCMB disruption on PRAS40 dimerization, as determined by GST pull-down assay. The pull-down amount of Venus-PRAS40 was normalized with that of GST-PRAS40. The data are presented as mean ± SEM ($n = 6$). (**F**) Dose–response curve of BRET^n signal from PRAS40 dimerization and NLuc-Venus upon 16-h treatment of pararosaniline. The final DMSO concentration was 2% (*v*/*v*) in samples with compound treatment. No significant change of BRET^n signal was observed in the presence of 2% DMSO for the period of compound treatment (data not shown). The data are presented as mean ± SEM from four replicates. *$P \leq 0.05$, **$P \leq 0.01$, ***$P \leq 0.001$.

As a proof-of-concept, proteins in the Hippo signaling pathway were examined with known interaction pairs as controls (Harvey et al., 2013; Johnson and Halder, 2014). As shown in Figure 7A, PPIs among proteins in the Hippo tumor suppressor pathway, including RASSF1, MST1, LATS2, YAP1, TEAD2, and 14-3-3ζ, were tested pair-wise using the uHTS BRET^n platform. BRET^n saturation curves were generated for each PPI pair (Figure 7B–J). Using AUC values as a quantitative measurement of PPI-induced BRET^n signal, a significant signal was detected for all known interactions in the Hippo pathway (Figure 7B–H). These PPI-induced BRET^n signals reached plateau at high concentration of acceptor protein, and were significantly higher (*P*-value ≤0.05) than background signals from empty NLuc or Venus controls (Figure 7B–H). The S/B ratio of AUC values was 15.3 for RASSF1/RASSF1 (Figure 7B) (Ortiz-Vega et al., 2002), 2.8 for RASSF1/MST1 (Figure 7C) (Hwang et al., 2007), 3.1 for MST1/MST1 (Figure 7D) (Creasy et al., 1996), 2.1 for MST1/LATS2 (Figure 7E) (Couzens et al., 2013), 2.8 for LATS2/YAP1 (Figure 7F) (Hao et al., 2008), 1.4 for YAP1/14-3-3ζ (Figure 7G) (Couzens et al., 2013), and 2.3 for YAP1/TEAD2 (Figure 7H) (Vassilev et al., 2001; Zhao et al., 2008). These results for known PPIs validate the specificity of the BRET^n platform in a uHTS format for efficient PPI monitoring in live cells, and determine the cutoff of 1.2 for identification of positive PPIs in the following studies.

In these studies, a total of 21 PPIs among core proteins in the Hippo pathway were examined from both directions of tag-fusion combinations. A heat map was constructed using the cutoff of 1.2, where 13 PPIs were considered positive with the S/B ratio of AUC values >1.2 and *P*-value ≤0.05 (Figure 7K). The rest of the protein pairs were considered negative for PPI, which is consistent with published results (Couzens et al., 2013; Kwon et al., 2013). All the raw data were also deposited in the CTD^2 Data Portal and Dashboard.

Interestingly, two new PPIs among Hippo pathway proteins were discovered, i.e. the LATS2/LATS2 homodimer (S/B of AUC 5.6, *P*-value ≤ 0.001; Figure 7I) and the RASSF1/LATS2 PPI (S/B of AUC 5.1, *P*-value ≤ 0.001; Figure 7J). The positive BRET^n signals obtained for each PPI pair support direct interaction within the protein pair, because of the stringent requirements for close proximity (≤10 nm) to obtain positive signals by this resonance energy transfer-based detection system. To validate these newly identified

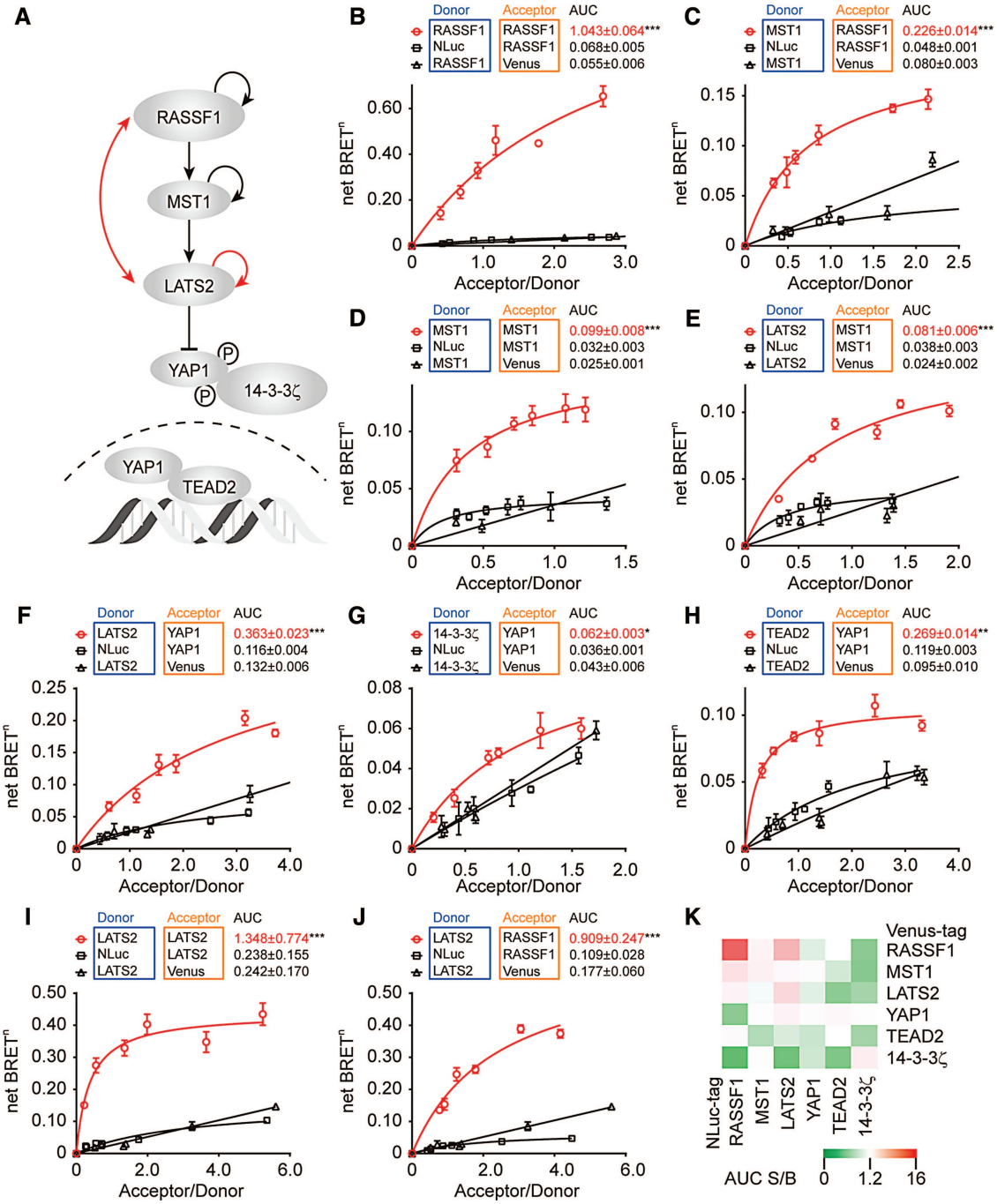

Figure 7 BRET^n mapping of binary PPIs among core Hippo pathway proteins. (**A**) Core Hippo pathway proteins. Known PPIs are indicated as black line connections, and unreported PPIs are indicated as red line connections. (**B**–**H**) BRET^n saturation curves of known PPIs reported in Hippo pathway. (**I**) BRET^n saturation curves of LATS2/LATS2 dimerization. (**J**) BRET^n saturation curves of RASSF1/LATS2 interaction. The data are expressed as mean ± SD from four replicates. AUC values for PPIs and highest background are listed and presented as mean ± SD from three independent experiments. *$P \leq 0.05$, **$P \leq 0.01$, ***$P \leq 0.001$. (**K**) Heat map of orthogonal PPI screening among Hippo pathway proteins. Colors are assigned according to the AUC FOC values with a cutoff of 1.2.

PPIs, GST pull-down was employed as a complementary confirmatory method. The GST-affinity chromatography (Figure 8A and B) gave rise to significantly higher signals for the PPI pairs than empty tag vector controls. The discovery and validation of these two PPIs provide new insights into the Hippo signaling network. For example, RASSF1 may serve as a scaffold to modulate the MST1–LATS2 signaling relay. These data strongly support the notion that our uHTS BRET^n platform can be utilized as an efficient tool to rapidly unveil unknown PPIs and advance the understanding of functional signaling circuitry in cells.

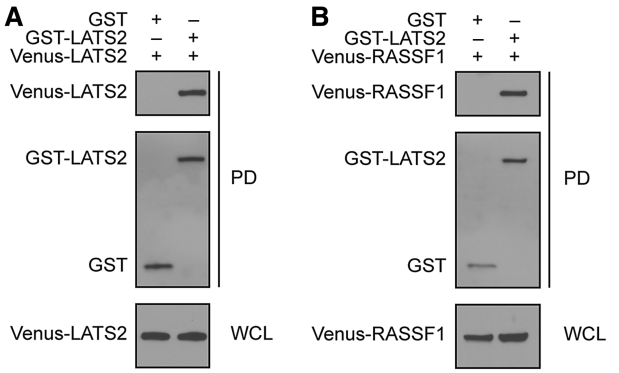

Figure 8 The validation of unreported PPIs of LATS2/LATS2 and LATS2/RASSF1 in Hippo pathway. GST pull-down validation of LATS2/LATS2 (**A**) and LATS2/RASSF1 (**B**) in HEK293T cells. $*P \leq 0.05$, $**P \leq 0.01$, $***P \leq 0.001$.

Discussion

With the BRET^n technology presented here, we demonstrate the feasibility of using NLuc/Venus as an effective BRET donor/acceptor pair. The high sensitivity of this donor/acceptor pair allows detection of PPIs among proteins at endogenous levels in live cells and enables miniaturization of BRET^n in a uHTS format in 1536-well plates. This miniaturized configuration allows streamlined operation, automated signal integration, pipelined analysis, and extensive titration to ensure high-quality data with consistent results.

The system is readily applicable for discovery of small-molecule PPI modulators. Using PRAS40 dimerization as an example, we demonstrated that the BRET^n assay has robust performance in uHTS format and is capable of detecting inhibitors of the PRAS40 interaction. One of the hit compounds from pilot screening, PCMB, is known for its disulfide activity, reacting with thiol groups on cysteine residues (Favrot et al., 2014). Identification of PCMB as the first-in-class PRAS40 dimerization disruptor suggests a potential mechanism of cysteine-mediated PRAS40 dimerization. PCMB could be further used as a tool compound to reveal the physiological significance and function of PRAS40 dimerization.

Further, the successful detection of known and unknown PPIs in our pilot binary PPI profiling for the Hippo pathway validated the utility of uHTS BRET^n for PPI network mapping. We revealed and validated two unreported new PPIs in the Hippo pathway (Couzens et al., 2013; Kwon et al., 2013), which suggests RASSF1 as a scaffold protein regulating Hippo signaling, leading to a revised Hippo signaling pathway model.

The developed BRET^n biosensors for various PPIs described in this study, including known and unknown PPIs, can be used as powerful tools for PPI functional interrogation in a uHTS format. For example, targeting the Hippo pathway has been suggested as a promising strategy in cancer therapy (Johnson and Halder, 2014). Each Hippo pathway PPI BRET^n biosensor can be readily applied as a validated and optimized uHTS platform for screening small-molecule PPI modulators that modulate Hippo pathway activity towards targeted cancer therapy, such as YAP/TEAD inhibitors. The miniaturized configuration also allows Hippo pathway profiling to monitor the activity of multiple PPIs along the defined pathway in a single plate.

BRET has been used to quantitatively study PPIs, such as G protein-coupled receptor dimerization (Ayoub et al., 2002; Mercier et al., 2002). One of the key features allowing PPI quantification is normalization of the BRET signal with protein expression levels to achieve relatively quantitative interpretation of PPI affinity ($BRET_{50}$) and amount ($BRET_{max}$). Herein, the power of the quantitative capability of BRET^n technology for studying PPIs in live cells was validated using a known model system of differential binding of Raf-1 with 14-3-3σ WT and K49E (Figure 3A), and this result further confirmed the previous studies showing the importance of the K49 residue in mediating the 14-3-3σ/Raf-1 interaction. In contrast, other high-throughput PPI detection platforms, such as yeast two-hybrid, protein fragment complementation assay, and affinity purification-coupled mass spectrometry, intrinsically lack the ability to readily monitor expression levels of test proteins that are directly correlated with PPI signal, and may complicate quantitative interpretation of PPI signals. Some other PPI detection methods mostly using purified proteins can only quantitatively assess PPI *in vitro* in a low-throughput fashion (Meyerkord and Fu, 2015). These highlight the critical importance of developing a high-throughput PPI detection method with streamlined protein expression monitoring in living cells for quantitative assessment of PPIs in physiologically relevant conditions.

Recently, NLuc was used as BRET donor, coupled with substrate-labeled Halo Tag-fused protein acceptor (Machleidt et al., 2015). This configuration allows a wide range of applications. However, it is not straightforward to characterize acceptor expression without additional washing steps. A major advantage of BRET^n is its simplicity to quantitatively measure PPIs by normalizing the BRET signal over the expression level of both donor and acceptor proteins. The BRET signal and protein expression levels can be simply acquired through monitoring the luminescence and fluorescence activity of genetically fused NLuc and Venus in parallel in an add-and-read mode without additional manipulation.

The current study utilized HEK293T cells for development and optimization of the BRET^n technology platform. However, simple setup of co-expressing exogenous NLuc- and Venus-tagged proteins and high sensitivity for detecting PPIs at low expression levels in live cells will significantly expand the utility of BRET^n for profiling various pathways in multiple cellular contexts. Desired cell lines either transiently or stably co-transfected with NLuc- and Venus-tagged proteins of interest will be valuable tools for systems biology studies and drug discovery. The use of cell lines with defined genomic backgrounds, such as oncogenic activation with mutated KRas, amplified c-Myc, or inactivation of tumor suppressors such as TP53 and Rb1, may allow the discovery and interrogation of disease-associated PPI pathways for developing therapeutic strategies.

In summary, we have developed a NLuc-based BRET^n technology, termed BRET^n. We have demonstrated robust performance of NanoLuc/Venus as a BRET donor/acceptor pair to study dynamic PPIs in living cells with high specificity and selectivity. The significantly enhanced sensitivity of BRET^n enabled the

detection of PPIs, as well as discovery of PPI modulators, at nearly endogenous expression level in 1536-well uHTS format. BRET^n has been applied in the discovery of the first inhibitor of PRAS40 dimerization and two novel PPIs, LATS2/LATS2 and RASSF1/LATS2, in the Hippo signaling pathway. Future application of BRET^n will enable quantitative PPI network mapping in physiologically relevant cellular environments. Established biosensors for 14 distinct PPIs as reported herein can be readily utilized for protein interaction studies and chemical probe discovery.

Materials and methods

Plasmids

The Gateway cloning system (Invitrogen) was used to generate the mammalian expression plasmids containing the gene cDNAs with a NLuc-, RLuc-, or Venus-tag at the 5′ end. In all cases, a 10-amino acid flexible linker sequence ($(Gly_4Ser)_2$) was inserted between the tag and coding cDNA. The pDONR vectors with the gene cDNAs were either purchased from DNASU or cloned by PCR. All plasmids generated were confirmed by sequencing. The vector backbones are pDEST26 vector (Invitrogen) for NLuc- and RLuc-tag constructs and pFUW vector for Venus-tag constructs. All expression vectors used in this study are listed in Table 1.

Cell culture

Human non-small cell lung carcinoma H1299 cells (ATCC, Manassas, VA; CRL-5803) were maintained in RPMI-1640 medium, supplemented with 10% fetal bovine serum and 1× penicillin/streptomycin solution (CellGro). HEK293T cells (ATCC) were maintained in Dulbecco's Modified Eagle's Medium (DMEM), supplemented with 10% fetal bovine serum and 1× penicillin/streptomycin solution (CellGro). Cells were incubated at 37°C in humidified conditions with 5% CO_2.

Table 1 List of expression vectors.

Vector name	Common gene name	HGCN ID
pDEST26-NLuc-HA-SFN	*14-3-3SIGMA*	HGNC:10773
pDEST26-NLuc-HA-YWHAZ	*14-3-3ZETA*	HGNC:12855
pDEST26-NLuc- HA-CDK6	*CDK6*	HGNC:1777
pDEST26-NLuc-HA-CDKN2B	*CDKN2B*	HGNC:1788
pDEST26-NLuc-HA-PRAS40	*PRAS40*	HGNC:28426
pDEST26-NLuc-HA-TP53	*TP53*	HGNC:11998
pDEST26-NLuc-HA-MDM2	*MDM2*	HGNC:6973
pDEST26-NLuc-HA-RASSF1	*RASSF1*	HGNC:9882
pDEST26-NLuc-HA-MST1	*MST1*	HGNC:11408
pDEST26-NLuc-HA-LATS2	*LATS2*	HGNC:6515
pDEST26-NLuc-HA-YAP1	*YAP1*	HGNC:16262
pDEST26-NLuc-HA-TEAD2	*TEAD2*	HGNC:11715
pFUW-Venus-FLAG-14-3-3SIGMA	*14-3-3SIGMA*	HGNC:10773
pFUW-Venus-FLAG-14-3-3ZETA	*14-3-3ZETA*	HGNC:12855
pFUW-Venus-FLAG-CDK6	*CDK6*	HGNC:1777
pFUW-Venus-FLAG-CDKN2B	*CDKN2B*	HGNC:1788
pFUW-Venus-FLAG-PRAS40	*PRAS40*	HGNC:28426
pFUW-Venus-FLAG-TP53	*TP53*	HGNC:11998
pFUW-Venus-FLAG-MDM2	*MDM2*	HGNC:6973
pFUW-Venus-FLAG-RASSF1	*RASSF1*	HGNC:9882
pFUW-Venus-FLAG-MST1	*MST1*	HGNC:11408
pFUW-Venus-FLAG-LATS2	*LATS2*	HGNC:6515
pFUW-Venus-FLAG-YAP1	*YAP1*	HGNC:16262
pFUW-Venus-FLAG-TEAD2	*TEAD2*	HGNC:11715

Forward transfection in a 1536-well plate format for uHTS

Linear polyethylenimines (PEIs, Polysciences, PA Cat # 23966) were used as transfection reagent throughout the study for forward transfection in 1536-well plates. Briefly, 4 μl of cell suspension (1000 cells/well for H1299 and 2000 cells/well for HEK293T cells) was dispensed into a 1536-well plate using a Multidrop^{TM} Combi Dispenser (Thermo-Fisher Scientific). After incubating for 24 h, 1 μl of DNA/PEI containing a total of 10 ng of desired plasmids and 30 ng PEI mixed in cell culture media was added directly into the 1536-well cell plate using a 384-cannula array integrated with Sciclone ALH 3000 liquid handler (PerkinElmer). Each sample was tested with four replicates. Two sets of 1536-well plates, one white plate (Corning, Cat # 3727) for BRET signal measurement and another black plate (Corning, Cat # 3893) for the measurement of Venus fluorescence intensity, were prepared side-by-side.

Luminescence spectrum scanning

H1299 cells (4000 cells in 45 μl per well) were plated in 384-well white cell culture plates (Corning, Cat # 3570). After 24 h incubation, cells were transiently transfected with 5 μl of DNA/PEI mixture containing a total of 50 ng desired plasmids (NLuc- or RLuc-tagged plasmids alone or in combination with Venus-tagged plasmids) and 150 ng PEI. Forty-eight hours after transfection, 10 μl of luminescence substrates [Furimazine (Nano-Glo, 1:600, Promega, Cat # N1120) or ViviRen^{TM} (60 μM, Promega, Cat # E6492)] were added directly to the cells. The luminescence spectrum from live cells was then scanned using a SpectraMax M2e Multi-Mode Microplate Reader (Molecular Devices).

BRET^n measurement

BRET^n signal measurements were performed 48 h after transfection. Cells were plated in a 1536-well plate and incubated for 24 h. For quantitative assessment of PPI formation, a BRET saturation assay was performed. Briefly different amounts of NLuc-tagged donor plasmid (0.025–0.25 ng/well) and Venus-tagged acceptor plasmid (0.5–10 ng/well), alone or in combination at various donor/acceptor ratios, were transfected as described above. After 48 h incubation, the cell permeable NLuc luciferase substrate, furimazine was added to the cells directly. The donor luminescence signal at 460 nm and acceptor emission signal at 535 nm were measured immediately using an Envision Multilabel plate reader (PerkinElmer).

The BRET^n signal is expressed as the ratio of light intensity measured at 535 nm over that at 460 nm. The specific BRET^n signal for the interaction of two proteins is expressed as net BRET^n, which is defined as the difference in BRET signal with co-expression of two proteins and expression of the negative control NLuc-protein only.

Measurement of donor and acceptor protein expression

The relative amount of NLuc-donor protein expression was measured by the luminescence signal at 460 nm (L_{460}) during the BRET^n signal measurement in 1536-well white plate; while the Venus acceptor protein expression was detected by the Venus fluorescence intensity (FI) with excitation at 480 nm and emission

at 535 nm in 1536-well black clear-bottom plate. Cells were seeded and transfected side-by-side under the same conditions for the 1536-well white plate for BRET^n measurement and black plate for Venus FI measurement. The ratio of relative amount of acceptor over donor protein expression (Acceptor/Donor) was defined as Venus FI/L_{460}. This intensity ratio should be proportional to the acceptor/donor ratio.

Data analysis

The BRET^n saturation curve was established using GraphPad Prism, based on the equation

$$Y = \frac{\text{BRET}_{\max} \cdot X}{\text{BRET}_{50} + X},$$

where Y is net BRET^n, and X is Acceptor/Donor. For quantitative analysis of the BRET^n assay, the area under the curve (AUC) was computed as a measurement of BRET^n signal, as AUC integrates both the amplitude and shape of the BRET signal curve for each PPI (Basu et al., 2013). The AUC values for signal and background controls were calculated using MatLab. The signal-to-background ratio (S/B) of the AUC was calculated using the overlapped X values of signal and background. The negative X and Y values were excluded from the analysis. The statistical significance of the difference between the signal and background was calculated using the rank sum permutation test in MatLab. P-values of 0.05 or less were considered statistically significant.

uHTS BRET^n system for small-molecule PPI modulator screening

HEK293T cells were plated and transfected with NLuc-PRAS40 (0.025 ng/well) and Venus-PRAS40 (2.5 ng/well) in 1536-well plate as described. After 24 h incubation, compounds (LOPAC, Sigma-Aldrich and part of NCI diversity compound library) were added to cells at a final concentration of 20 μM. After 16 h compound treatment, BRET signal was measured as described above. Each compound was tested in quadruplicate. Z' factor was calculated as

$$Z' = 1 - \frac{3 \times \text{SD}_{\text{PPI}} + 3 \times \text{SD}_{\text{NLuc-PRAS40}}}{\text{BRET signal}_{\text{PPI}} - \text{BRET signal}_{\text{NLuc-PRAS40}}},$$

where SD_{PPI} and $\text{SD}_{\text{NLuc-PRAS40}}$ are the standard deviations of the BRET signal for cells transfected with NLuc-PRAS40 plus Venus-PRAS40 and NLuc-PRAS40 plus empty Venus, respectively; BRET $\text{signal}_{\text{PPI}}$ and BRET $\text{signal}_{\text{NLuc-PRAS40}}$ are the corresponding mean BRET signals for PRAS40 dimerization and NLuc-PRAS40 only, respectively. A Z' factor between 0.5 and 1.0 indicates that the assay is suitable for HTS (Zhang et al., 1999). The final DMSO concentration was 2% (v/v) for compound screening.

GST pull-down

HEK293T cells were seeded in 6-well plates at 200000 cells/well in 2 ml medium. After 24 h incubation, 1 μg of GST-tagged and 1 μg of Venus-FLAG-tagged plasmids were transfected into the cells using PEI. Forty-eight hours after transfection, cells were lysed in 1% NP-40 buffer (150 mM NaCl, 10 mM HEPES (pH 7.5), 1% NP-40, 5 mM sodium pyrophosphate, 5 mM NaF, 2 mM sodium orthovanadate, 10 mg/L aprotinin, 10 mg/L leupeptin, and 1 mM PMSF). Lysates were incubated with glutathione-conjugated beads (GE) for 2 h at 4°C. Beads were washed three times with 1% NP-40 buffer and eluted by boiling in sodium dodecyl sulfate-polyacrylamide gel electrophoresis (SDS-PAGE) loading buffer and subjected to western blot analysis.

Western blotting

The following primary antibodies were used: rabbit anti-PRAS40 (IBL); rabbit anti-GST (Santa Cruz Biotechnology, sc-459); mouse anti-Flag (Sigma, M2).

Acknowledgements

We would like to thank members of the Fu laboratory for helpful discussions and Dr Maggie Johns (Department of Pharmacology and Emory Chemical Biology Discovery Center) for valuable comments and editing.

Funding

This study is supported in part by National Cancer Institute to H.F., Y.D., and F.R.K. (NIH U01CA168449) and to the Winship Cancer Institute of Emory University (NIH 5P30CA138292).

Conflict of interest: none declared.

References

Angers, S., Salahpour, A., Joly, E., et al. (2000). Detection of β_2-adrenergic receptor dimerization in living cells using bioluminescence resonance energy transfer (BRET). Proc. Natl Acad. Sci. USA *97*, 3684–3689.

Ayoub, M.A., Couturier, C., Lucas-Meunier, E., et al. (2002). Monitoring of ligand-independent dimerization and ligand-induced conformational changes of melatonin receptors in living cells by bioluminescence resonance energy transfer. J. Biol. Chem. *277*, 21522–21528.

Basu, A., Bodycombe, N.E., Cheah, J.H., et al. (2013). An interactive resource to identify cancer genetic and lineage dependencies targeted by small molecules. Cell *154*, 1151–1161.

Canals, M., Marcellino, D., Fanelli, F., et al. (2003). Adenosine A_{2A}-Dopamine D_2 receptor-receptor heteromerization: qualitative and quantitative assessment by fluorescence and bioluminescence energy transfer. J. Biol. Chem. *278*, 46741–46749.

Cancer Genome Atlas Research Network. (2008). Comprehensive genomic characterization defines human glioblastoma genes and core pathways. Nature *455*, 1061–1068.

Cancer Genome Atlas Research Network. (2014a). Comprehensive molecular characterization of urothelial bladder carcinoma. Nature *507*, 315–322.

Cancer Genome Atlas Research Network. (2014b). Comprehensive molecular profiling of lung adenocarcinoma. Nature *511*, 543–550.

Cancer Genome Atlas Research Network. (2014c). Integrated genomic characterization of papillary thyroid carcinoma. Cell *159*, 676–690.

Collins, B.C., Gillet, L.C., Rosenberger, G., et al. (2013). Quantifying protein interaction dynamics by SWATH mass spectrometry: application to the 14-3-3 system. Nat. Methods *10*, 1246–1253.

Couturier, C., and Deprez, B. (2012). Setting up a bioluminescence resonance energy transfer high throughput screening assay to search for protein/protein interaction inhibitors in mammalian cells. Front. Endocrinol. *3*, 1–13.

Couzens, A.L., Knight, J.D., Kean, M.J., et al. (2013). Protein interaction network of the mammalian Hippo pathway reveals mechanisms of kinase-phosphatase interactions. Sci. Signal. *6*, rs15.

Creasy, C.L., Ambrose, D.M., and Chernoff, J. (1996). The Ste20-like protein kinase, Mst1, dimerizes and contains an inhibitory domain. J. Biol. Chem. *271*, 21049–21053.

Ding, Z., Liang, J., Lu, Y., et al. (2006). A retrovirus-based protein complementation assay screen reveals functional AKT1-binding partners. Proc. Natl Acad. Sci. USA *103*, 15014–15019.

Favrot, L., Lajiness, D.H., and Ronning, D.R. (2014). Inactivation of the Mycobacterium tuberculosis antigen 85 complex by covalent, allosteric inhibitors. J. Biol. Chem. *289*, 25031–25040.

Fu, H., Subramanian, R.R., and Masters, S.C. (2000). 14-3-3 proteins: structure, function, and regulation. Annu. Rev. Pharmacol. Toxicol. *40*, 617–647.

Hall, M.P., Unch, J., Binkowski, B.F., et al. (2012). Engineered luciferase reporter from a deep sea shrimp utilizing a novel imidazopyrazinone substrate. ACS Chem. Biol. *7*, 1848–1857.

Hamdan, F.F., Audet, M., Garneau, P., et al. (2005). High-throughput screening of G protein-coupled receptor antagonists using a bioluminescence resonance energy transfer 1-based β-arrestin2 recruitment assay. J. Biomol. Screen. *10*, 463–475.

Hannon, G.J., and Beach, D. (1994). p15INK4B is a potential effector of TGF-beta-induced cell cycle arrest. Nature *371*, 257–261.

Hao, Y.W., Chun, A., Cheung, K., et al. (2008). Tumor suppressor LATS1 is a negative regulator of oncogene YAP. J. Biol. Chem. *283*, 5496–5509.

Harvey, K.F., Zhang, X., and Thomas, D.M. (2013). The Hippo pathway and human cancer. Nat. Rev. Cancer *13*, 246–257.

Havel, J.J., Li, Z., Cheng, D., et al. (2015). Nuclear PRAS40 couples the Akt/mTORC1 signaling axis to the RPL11-HDM2-p53 nucleolar stress response pathway. Oncogene *34*, 1487–1498.

Huang, J., Wu, S., Barrera, J., et al. (2005). The Hippo signaling pathway coordinately regulates cell proliferation and apoptosis by inactivating Yorkie, the Drosophila homolog of YAP. Cell *122*, 421–434.

Hwang, E., Ryu, K.S., Paakkonen, K., et al. (2007). Structural insight into dimeric interaction of the SARAH domains from Mst1 and RASSF family proteins in the apoptosis pathway. Proc. Natl Acad. Sci. USA *104*, 9236–9241.

Johnson, R., and Halder, G. (2014). The two faces of Hippo: targeting the Hippo pathway for regenerative medicine and cancer treatment. Nat. Rev. Drug Discov. *13*, 63–79.

Kwon, Y., Vinayagam, A., Sun, X., et al. (2013). The Hippo signaling pathway interactome. Science *342*, 737–740.

Machleidt, T., Woodroofe, C.C., Schwinn, M.K., et al. (2015). NanoBRET-A novel BRET platform for the analysis of protein-protein interactions. ACS Chem. Biol. *10*, 1797–1804.

Mercier, J.F., Salahpour, A., Angers, S., et al. (2002). Quantitative assessment of β_1- and β_2-adrenergic receptor homo- and heterodimerization by bioluminescence resonance energy transfer. J. Biol. Chem. *277*, 44925–44931.

Meyerkord, C., and Fu, H. (2015). Protein-Protein Interactions: Methods and Applications. Totowa: Humana Press.

Ortiz-Vega, S., Khokhlatchev, A., Nedwidek, M., et al. (2002). The putative tumor suppressor RASSF1A homodimerizes and heterodimerizes with the Ras-GTP binding protein Nore1. Oncogene *21*, 1381–1390.

Pfleger, K.D.G., and Eidne, K.A. (2006). Illuminating insights into protein-protein interactions using bioluminescence resonance energy transfer (BRET). Nat. Methods *3*, 165–174.

Ramsay, D., Kellett, E., McVey, M., et al. (2002). Homo- and hetero-oligomeric interactions between G-protein-coupled receptors in living cells monitored by two variants of bioluminescence resonance energy transfer (BRET): hetero-oligomers between receptor subtypes form more efficiently than between less closely related sequences. Biochem. J. *365*, 429–440.

Rolland, T., Tasan, M., Charloteaux, B., et al. (2014). A proteome-scale map of the human interactome network. Cell *159*, 1212–1226.

Tarassov, K., Messier, V., Landry, C.R., et al. (2008). An in vivo map of the yeast protein interactome. Science *320*, 1465–1470.

Vassilev, A., Kaneko, K.J., Shu, H., et al. (2001). TEAD/TEF transcription factors utilize the activation domain of YAP65, a Src/Yes-associated protein localized in the cytoplasm. Genes Dev. *15*, 1229–1241.

Vassilev, L.T., Vu, B.T., Graves, B., et al. (2004). In vivo activation of the p53 pathway by small-molecule antagonists of MDM2. Science *303*, 844–848.

Vrecl, M., Jorgensen, R., Pogacnik, A., et al. (2004). Development of a BRET^2 screening assay using β-arrestin 2 mutants. J. Biomol. Screen. *9*, 322–333.

Xu, Y., Piston, D.W., and Johnson, C.H. (1999). A bioluminescence resonance energy transfer (BRET) system: application to interacting circadian clock proteins. Proc. Natl Acad. Sci. USA *96*, 151–156.

Zhang, J.H., Chung, T.D., and Oldenburg, K.R. (1999). A simple statistical parameter for use in evaluation and validation of high throughput screening assays. J. Biomol. Screen. *4*, 67–73.

Zhao, B., Wei, X., Li, W., et al. (2007). Inactivation of YAP oncoprotein by the Hippo pathway is involved in cell contact inhibition and tissue growth control. Genes Dev. *21*, 2747–2761.

Zhao, B., Ye, X., Yu, J., et al. (2008). TEAD mediates YAP-dependent gene induction and growth control. Genes Dev. *22*, 1962–1971.